Analysis of elastic and inelastic scattering of ^{20}Ne on ^{76}Ge at 306 MeV

A. Hemmdan,[1,2,*] M. A. Hassanain,[3] M. Anwar,[1,2] and Kassem O. Behairy[1,2]
[1]*Department of Physics, Aswan University, Aswan 81528, Egypt*
[2]*Academy of Scientific Research and Technology (ASRT), Cairo 11516, Egypt*
[3]*Department of Physics, New-Valley University, El-Kharga 72511, Egypt*

(Received 16 May 2021; accepted 23 August 2021; published 6 October 2021)

Angular distributions of the differential cross section for ^{20}Ne + ^{76}Ge elastic and inelastic scattering at energy 306 MeV are analyzed in the framework of the optical model. The analysis is performed using the coupled-channels mechanism by taking into account the effect of the low-lying states, 0^+ and 2^+ for the projectile ^{20}Ne ($E_{\text{ex.}} = 1.634$ MeV), target ^{76}Ge ($E_{\text{ex.}} = 0.563$ MeV) nuclei, and their mutual excitation (2^+, 2^+). Results are obtained with the conventional phenomenological Woods-Saxon potential and three different semimicroscopic potentials using the double folding model. Two real cluster potential models are calculated based upon the cluster structure of ^{20}Ne nucleus as 5α and $\alpha + {}^{16}$O. For the sake of comparison, the real of the density-energy-dependent CDM3Y6 potential is considered. The imaginary part for the three real potentials is treated in a standard Woods-Saxon form. The calculations show that the experimental data can be reproduced successfully with a scale factor close to 1. The coupled channels have a weak effect on the elastic scattering with significant differences in calculations of the volume integrals and the total reaction cross sections compared to the available previous study for this reaction. Other future studies are, therefore, required.

DOI: 10.1103/PhysRevC.104.044604

I. INTRODUCTION

The ambiguous question of whether the neutrinos are Majorana fermions is still unsolved. The neutrinoless double β decay ($0\nu\beta\beta$) if observed it will be the most promising resource to establish the Majorana or Dirac nature of neutrino and would provide a precise measurement of its absolute mass.

Recent projects [1–4] focus on nuclear single and double charge exchange (DCE) nuclear reactions. Their aim is to extract relevant information for the $0\nu\beta\beta$ nuclear matrix element (NME) from the study of DCE reaction cross sections.

Therefore, the scope of the present paper focuses on the DCE reactions due to their large current interest, and the investigation of their initial- and final-state interactions becomes of crucial importance to understand their precise reaction mechanisms. One of these pertinent reactions is the ^{20}Ne + ^{76}Ge DCE reaction as ^{76}Ge considers one of the most promising candidates for direct observation of the $0\nu\beta\beta$ mode [1]. The analysis of the elastic and inelastic channels of the ^{20}Ne + ^{76}Ge system is of particular interest for the cross section of the ^{76}Ge(^{20}Ne ,^{20}O) ^{76}Se DCE that is performed within the NUMEN project [1,2] since the proposed approach to get information about NMEs of interest for $0\nu\beta\beta$ within NUMEN is a multichannel one. The study of the weak-interaction considerations is out of the scope of the present paper.

For the first time, elastic and inelastic scattering angular distributions for the ^{20}Ne + ^{76}Ge system at 306-MeV laboratory energy were measured [5], and the calculations are analyzed within the optical model plus distorted-wave Born approximation and coupled channel (CC) approaches. They used three different optical potential (OP) models to describe the elastic angular distribution. The three chosen OPs failed to describe the elastic scattering experimental data above the grazing angle (≈9.4°). This result led them to confirm that the theoretical description of elastic scattering is not strongly dependent on the choice of the OP. They also studied the CC effects which are found to be essential to obtain good agreement with the experimental data. They concluded that new analyses have to be performed to find the appropriate characterization of the model space and average interaction for the outgoing partition.

During the past three decades, the double folding (DF) model has been widely used to calculate the real part of nucleus-nucleus OP due to its simple handling in numerical calculations to carry out a variety of analyses of heavy-ion (HI) scattering [6]. The basic inputs of the DF calculations are the nuclear densities of the colliding nuclei and effective nucleon-nucleon (NN) interaction. One of the popular choices for the NN interactions is the M3Y interaction [7]. This original density-independent M3Y interaction is developed [8] to include the density dependent (DD) in the nucleon OP which leads to saturating the cold nuclear matter (NM) to collapse. Afterward, several forms of M3Y density dependences were introduced [9,10] with chosen parameter values to reproduce the observed NM saturation properties. The DD of the M3Y denoted by CDM3Yn ($n = 1 \rightarrow 6$) is allowed to infer the values of nuclear incompressibility with more precision than the other different DD versions. The effective CDM3Y6 interaction has been widely tested in the DF model analyses

*ahemdan@aswu.edu.eg

of the elastic nucleus-nucleus scattering [9–13]. Therefore, this version of NN interaction is adopted in the present paper.

On the other hand, several studies have been carried out to investigate the DF cluster potentials based upon the α-cluster structure of the colliding nuclei in the analyses of α-nucleus and nucleus-nucleus elastic scattering [14–19]. The structure of ^{20}Ne has been earlier also studied by various models which are almost based on the description of the motion of nucleons in the nucleus [20].

In Ref. [21], ^{20}Ne is considered to be composed of two clusters a core ^{16}O and an extra α particle. They obtained a successful description for the elastic scattering of 800-MeV protons by ^{20}Ne nucleus.

The same visualization of the cluster structure for ^{20}Ne is adopted [22]. The authors presented an analytical deduction for the wave function for the relative motion of the $\alpha + {}^{16}$O system, and they succeeded very well to reproduce the experimental charge form factor of ^{20}Ne and the elastic proton $+ {}^{20}$Ne scattering differential cross sections.

Thereafter, a series of studies [23–25] provided support to two-cluster ($\alpha + {}^{16}$O) model of ^{20}Ne. For example, the folding potential for the elastic $\alpha + {}^{20}$Ne scattering [23], a satisfactory description for elastic scattering angular distributions for a wide incident energy region was obtained. Also, the authors in Ref. [24] construct an α-folding potential for the analysis of elastic $^{16}\mathrm{O} + {}^{20}$Ne scattering system in the energy range of $E_{\mathrm{c.m.}} = 24.5$–35.5 MeV. They aimed to further examine the two-cluster model of the ^{20}Ne nucleus. The experimental data have been reasonably well described using the α-folding potential with an imaginary potential consisting of a Woods-Saxon (WS) volume plus a derivative WS (WSD) surface term. Moreover, the two-cluster model of the ^{20}Ne nucleus is applied again to investigate its validity to get information about the analysis of the elastic $^{20}\mathrm{Ne} + {}^{20}$Ne scattering [25] at energies of 62.1–74.5 MeV.

The motivation of the present paper is due to the limited study of the $^{20}\mathrm{Ne} + {}^{76}$Ge interaction in conjunction with its features which have not been well established yet. Furthermore, these data may provide opportunities to test various scattering theories and nuclear-structure models. Therefore, our aim in this paper is to reexamine the two-cluster model in addition to the α cluster (5α cluster) of ^{20}Ne to present a description of the experimental data for $^{20}\mathrm{Ne} + {}^{76}$Ge elastic and inelastic scattering [5]. For the sake of comparison, we tested the DF potential using the CDM3Y6 effective NN interaction, which is dependent on the density and energy and proved to be effective in most folding calculations. Finally, for a complete understanding of the scattering dynamics of the studied reaction, the relevant internal states of the projectile-target system are properly taken into account. Therefore, the CC method is performed to describe the experimental cross-section angular distributions extracted for the elastic and some inelastic transitions.

This paper is organized as follows: A brief description of the derived formalisms and the procedures are given in Secs. II and III, respectively. Section IV is devoted to the results and discussion. Finally, conclusions are reported in Sec. V.

II. THEORETICAL FORMALISM

A. Elastic scattering

Four OP forms are used to calculate the nuclear potential for $^{20}\mathrm{Ne} + {}^{76}$Ge elastic scattering in the present paper. The form of the total nuclear potential is taken as

$$U(R) = V_{\mathrm{C}}(R) + U_{\mathrm{N}}(R), \tag{1}$$

where the Coulomb potential $V_{\mathrm{C}}(R)$ is taken as a uniformly charged sphere of radius $R_{\mathrm{C}} = 1.2\,(A_T^{1/3} + A_P^{1/3})$. A_T and A_P are the masses of the target and the projectile, respectively.

Phenomenologically, the nuclear OP part $U_{\mathrm{N}}(R)$ is taken in the form of WS shape,

$$U_{\mathrm{N}}(R) = V_0\left[1 + \exp\left(\frac{R - R_{\mathrm{V}}}{a_{\mathrm{V}}}\right)\right]^{-1} + iW_0\left[1 + \exp\left(\frac{R - R_{\mathrm{W}}}{a_{\mathrm{W}}}\right)\right]^{-1}, \tag{2}$$

where the first term represents the real part of OP whereas the second term represents the imaginary part. The parameters, $V_0(W_0)$, $R_{\mathrm{V}}(R_{\mathrm{W}})$, and $a_{\mathrm{V}}(a_{\mathrm{W}})$ are the depth, radius and diffuseness of the real (imaginary) potential, respectively. The radius is calculated according to $R_x = r_x\,(A_T^{1/3} + A_P^{1/3})$, $x = V,\ W$. This potential is denoted as WSP.

Semimicroscopically, the OP is generated when the imaginary part is taken as WS potential of Eq. (2) while the real part is calculated by using the DF model form:

$$V(R) = N_R \iint \rho_{\mathrm{Ne}}(\mathbf{r}_1)\rho_{\mathrm{Ge}}(\mathbf{r}_2)\, v_{\mathrm{NN}}(s)d\mathbf{r}_1 d\mathbf{r}_2, \qquad s = \mathbf{R} - \mathbf{r}_1 + \mathbf{r}_2, \tag{3}$$

where N_R is the real normalization factor. Three different forms of the real DF potentials are generated.

In the first one, we consider the two-cluster structure of the ^{20}Ne nucleus as $\alpha + {}^{16}$O, and this potential for the $^{20}\mathrm{Ne} + {}^{76}$Ge scattering is denoted as CP1. So, the real DF potential model is calculated as

$$V_{\mathrm{CP1}}(R) = N_R \int \left[V_{\alpha\text{-Ge}}\left(\mathbf{R} - \frac{4}{5}\mathbf{r}\right) + V_{\text{O-Ge}}\left(\mathbf{R} + \frac{1}{5}\right)\mathbf{r}\right] \times |\psi(r)|^2 d\mathbf{r}, \tag{4}$$

where $\psi(r)$ is the wave function for the relative motion of the α and ^{16}O clusters in the ground state (g.s.) of the ^{20}Ne nucleus, and $\mathbf{r}$ is the relative coordinate between the centers of mass (c.m.) of α and ^{16}O. The α-^{76}Ge interaction potential may be formulated as

$$V_{\alpha\text{-Ge}}(r) = \int \rho_{\mathrm{Ge}}(\mathbf{r}')v_{\alpha\mathrm{N}}(\mathbf{r} - \mathbf{r}')d\mathbf{r}'. \tag{5}$$

The effective $v_{\alpha\mathrm{N}}$ interaction is taken in a Gaussian form as [17]

$$v_{\alpha\mathrm{N}}(r) = -36.4e^{-0.2657r^2}. \tag{6}$$

The ^{16}O - ^{76}Ge interaction potential is formulated as

$$V_{\text{O-Ge}}(r) = \int \rho_{\mathrm{O}}(\mathbf{r}_1)\rho_{\mathrm{Ge}}(\mathbf{r}_2)v_{\mathrm{NN}}(s)d\mathbf{r}_1 d\mathbf{r}_2,$$

TABLE I. Parameters of the colliding nuclear densities of ^{20}Ne and ^{76}Ge with its corresponding rms radius values comparable with experimental and previous calculations. Experimentally, obtained from $\langle r_m^2\rangle^{1/2} = \langle r_{\rm ch}^2\rangle^{1/2} - \langle r_p^2\rangle^{1/2}$.

Nucleus	ρ_0 (fm^{-3})	$r_c(w)$ fm(fm^{-2})	$a_c(\beta)$ fm(fm^{-2})	$\sqrt{\langle r_m^2\rangle}$ (fm)
		2pF density		
^{76}Ge	0.16715	4.54	0.578	4.12[a]
				4.0[b] [26]
^{20}Ne	0.153505	2.805	0.571	3.04[a]
				2.897[b] [26]
				2.722[c] [19]
		MG density		
^{20}Ne ^{16}O	0.1317	0.6457	0.3228	2.45[a]
α	0.4229	0.0	0.7024	2.72[c] [21]
^{20}Ne (5α)	0.0403	0.412	0.277	2.47[a]
				2.44[c] [19]

[a]Present calculation.
[b]Experimental.
[c]Previous calculation.

$$s = \mathbf{r} - \mathbf{r}_1 + \mathbf{r}_2. \tag{7}$$

The effective NN interaction [16] is defined as

$$v_{\rm NN}(s) = -20.97e^{-0.463s^2}. \tag{8}$$

The ground-state density distributions of the target ^{76}Ge nuclei is taken in 2pF [26] as

$$\rho_{\rm Ge}(r) = \rho_0\left[1 + \exp\left(\frac{r - r_{\rm c}}{a_{\rm c}}\right)\right]^{-1}, \tag{9}$$

whereas the nuclear matter density of ^{16}O is taken in modified Gaussian (MG) form as [14]

$$\rho_{\rm O}(r) = \rho_0(1 + \omega r^2)e^{-\beta r^2}. \tag{10}$$

The parameters of the 2pF and MG matter densities form with corresponding root mean square (rms) radii are listed in Table I. The relative motion wave-function $\psi(r)$ was formulated [22–25] and given as the following:

$$\psi(r) = R_0(r)Y_{00}(\theta, \phi), \tag{11}$$

and the form of the radial wave-function $R_0(r)$ can be abbreviated to be written as

$$R_0(r) = (\eta - \xi\, r^2)e^{-(1/2\alpha^2)r^2}, \tag{12}$$

since $\eta = 2(a^6\pi)^{-1/4}[\sin\frac{\theta}{2} + \frac{3}{2}\sqrt{\frac{2}{3}}\cos\frac{\theta}{2}]$ and $\xi = 2\sqrt{\frac{2}{3}}(a^6\pi)^{-1/4}\cos\frac{\theta}{2}$ with $a = 1.96$ and $\theta = 282.4^\circ$ are obtained [23] by fitting the experimental charge form factor of the ^{20}Ne nucleus.

In the second form, the projectile ^{20}Ne is visualized to be, such as an α cluster (5α) with the same procedure for $v_{\alpha N}$ and the target density of ^{76}Ge nuclei in Eq. (9), the CP2 is the denoted for this potential. Therefore, the real part in the present potential takes the form

$$V_{\rm CP2}(R) = N_R \iint \rho^{\rm C}_{\rm Ne}(\mathbf{r}_1)\rho_{\rm Ge}(\mathbf{r}_2)\, v_{\alpha N}(s)d\mathbf{r}_1 d\mathbf{r}_2,$$
$$s = \mathbf{R} - \mathbf{r}_1 + \mathbf{r}_2, \tag{13}$$

where, the cluster density $\rho^{\rm C}_{\rm Ne}(\mathbf{r}_1)$ of the ^{20}Ne nucleus as 5α is taken in the MG density form which is calculated using the same technique in Ref. [14]. Its parameters with the α-matter density distribution [$(\rho_\alpha(r) = \rho_0 e^{-\beta r^2}$] [27] are listed in Table I.

Finally, when both the target and the projectile are considered to be consist of nucleons and the choice of the NN interaction is crucial, the third semimicroscopic potential is calculated. In the present paper, the density-dependent version of CDM3Y6 interaction [28] is used. Then the DF model of nuclear OP will be in the form

$$V_{\rm CDM3Y6}(R) = N_{\rm R} \iint \rho_{\rm Ne}(\mathbf{r}_1)\rho_{\rm Ge}(\mathbf{r}_2)\, v_{\rm NN}({\rm s})\, d\mathbf{r}_1 d\mathbf{r}_2, \tag{14}$$

where $\rho_{\rm Ne}$ and $\rho_{\rm Ge}$ are the ground-state 2pF density distributions of the projectile and target. Their parameters are listed in Table I. More details about the density-dependent version of CDM3Y6 effective NN interaction is defined in Ref. [29].

B. Inelastic scattering

The nuclei ^{20}Ne and ^{76}Ge are well known to be strongly deformed and their low-lying states have a rotational nature, therefore, the calculations in the framework of the coupled-channels method are most adequate to describe the experimental data on the elastic and inelastic scattering.

Two OPs are used to analyze the inelastic ^{20}Ne + ^{76}Ge scattering cross sections for the low-lying 2^+ state ($E_{\rm ex.} = 0.563$ MeV) of the target ^{76}Ge nucleus, 2^+ state ($E_{\rm ex.} = 1.634$ MeV) of the projectile ^{20}Ne nucleus and the mutual excitation for two colliding nuclei $^{20}{\rm Ne}_{1.634}(2^+)$ and $^{76}{\rm Ge}_{0.563}(2^+)$ by using the CC technique (see Refs. [30,31]).

First, the deformed potential (DP) of the WSP is directly obtained as a derivative of the WSP potential for the multipolarity $\lambda \geqslant 2$. In the DP model, excitations of the nucleus with $\lambda \geqslant 2$ are characterized by a transition potential whose shape is independent of λ,

$$U^{\rm DP}_\lambda(r) = -\delta^U_\lambda dU(r)/dr, \tag{15}$$

since δ^U_λ is the potential deformation length that determines the strength of the interaction.

The second model is the nuclear transition for potential CP1. The real transition potential, denoted as $U^{\rm tr(CP1)}_\lambda(r)$ can be written as

$$U^{\rm tr(CP1)}_\lambda(r) = N_R \iint \rho^{\rm tr}_{\rm Ne}(\mathbf{r}_1)\rho^{\rm tr}_{\rm Ge}(\mathbf{r}_2)\, v_{\rm NN}(s)d\mathbf{r}_1 d\mathbf{r}_2, \tag{16}$$

where $\rho^{\rm tr}_{\lambda(i)}(r)$ is the transition density which describes the inelastic excitation of the two colliding nuclei that derived according to the following:

$$\rho^{\rm tr}_{\lambda(i)}(r) = \delta^{\rm m}_\lambda d\rho_i(r)/dr, \quad i = {\rm Ne},\ {\rm Ge}, \tag{17}$$

since $\rho_i(r)$ is the ground-state density distribution of the projectile ^{20}Ne nucleus or the target ^{76}Ge nucleus. $\delta^{\rm m}_\lambda$ represents

TABLE II. The best-fit parameters which obtained for elastic scattering of the ^{20}Ne + ^{76}Ge system at 306 MeV. For the real part of WSP, $a_v = 0.964$ fm and $r_v = 0.77$ fm whereas the depth $W_0 = 84.3$ MeV is used for all imaginary potentials.

Pot.	V_0 (MeV)	J_R (MeV fm^3)	$\sqrt{\langle r_R^2 \rangle}$ (fm)	r_W (fm)	a_W (fm)	J_W (MeV fm^3)	$\sqrt{\langle r_W^2 \rangle}$ (fm)	χ^2	σ_R (mb)
WSP	288.7	270.5	5.92	1.048	0.94	104.5	6.63	3.0	3410
CP1	0.79	290.9	5.35	1.068	0.85	107.3	6.55	1.2	3209
CP2	0.7	257.7	5.5	1.13	0.723	120.9	6.63	2.2	3097
CDM3Y6	0.75	285.5	5.7	1.13	0.801	124.1	6.77	3.5	3344

$V_0 = N_R$ for the microscopic potential.

the matter deformation length which provides a measure of the nuclear transition rate. It can be obtained from the measured $B(E\lambda)$ transition rate. $\delta_\lambda^m = \beta_\lambda R$, where β_λ is the deformation parameter and R is the radius of the deformed nucleus ($R = 1.2A^{1/3}$ fm). The deformation parameter is determined by $\beta_\lambda = \frac{4\pi}{3ZR^2}[B(E\lambda; I \to I')\, b^2e^2/e^2]^{1/2}$. For the imaginary transition potential, the derivative of the imaginary central potential is obtained from

$$W_\lambda^i(r) = -\frac{1}{\sqrt{4\pi}}\delta_\lambda^w dW(r)/dr, \tag{18}$$

where δ_λ^w refers to the imaginary deformation length defined as $\delta_\lambda^w = \beta_\lambda^w R^i$, and β_λ^w is the imaginary deformation parameter.

According to Ref. [32], the equal deformation hypothesis for matter distribution and potential is, in fact, correct if the projectile is a pointlike particle and the potential is obtained by folding the density with a zero-range interaction. The correct deformation length (δ_λ^{corr}) is adopted for the deformed potential as in Ref. [33] to take into account the relative differences in the density and potential radii, as follows:

$$\delta_\lambda^{corr} = \delta_\lambda R/R_{pot}, \tag{19}$$

where the radius R_{pot} of the CP1 potential is listed in Table II.

In our calculations, we assume that the imaginary deformation length is equal to the matter deformation i.e., $\delta_\lambda^w = \delta_\lambda^{corr}$. Therefore, the corrected deformation lengths for ^{20}Ne are 1.43 fm which is consistent with Ref. [33] and 1.28 fm for ^{76}Ge is of the CP1 potential.

III. PROCEDURE

The analysis of ^{20}Ne + ^{76}Ge elastic scattering is performed based on the two-cluster approaches CP1 and CP2 as given by Eqs. (4) and (13), respectively. Furthermore, the DF real part of the OP is also evaluated using the CDM3Y6 density-energy-dependent effective NN interaction. The imaginary part of the OPs is calculated by Eq. (2) as a phenomenological WS volume form with three parameters.

The three considered real potentials given by the DFPD4 computer code [34] and our computer code [35] in addition to the fourth WS potential (WSP) are fed into HI-OPTIM-94 [36]. Searches were carried out using the HI-OPTM94 [36] computer code by optimizing four free parameters, the real renormalization factor N_R for the calculated potentials besides the parameters of the imaginary WS potentials to fit the data by minimizing the χ^2 value, defined as

$$\chi^2 = \frac{1}{N}\sum_{k=1}^{N}\left[\frac{\sigma_{th}(\theta_k) - \sigma_{ex}(\theta_k)}{\Delta\sigma_{ex}(\theta_k)}\right]^2. \tag{20}$$

$\sigma_{th}(\sigma_{ex})$ is the theoretical (experimental) cross section at an angle θ_k in the c.m. system, $\Delta\sigma_{ex}$ is the experimental error, and N is the number of the data points. For the experimental errors of all measured data, an average value of 10% is used. For the phenomenological WS approach in Eq. (2), searches are executed upon six free parameters for the elastic and inelastic scattering.

In the next step, only, two potentials WSP and CP1 are used to analyze inelastic ^{20}Ne + ^{76}Ge scattering, in the framework of the CC, at low-lying 2^+ state ($E_{ex.} = 0.563$ MeV) of the ^{76}Ge target nucleus and the low-lying 2^+ state ($E_{ex.} = 1.634$ MeV) of the ^{20}Ne projectile nucleus. The transition of the CP1 potential and the deformed WSP potential are generated to study the excited channels and their effect on ground channels. Therefore, the complex inelastic OP will be in the form

$$U_{trans}^{\lambda}(R) = V_\lambda^C(R) + U_\lambda^{N(WSP,\ CP1)}(R). \tag{21}$$

The inelastic angular distribution fits are obtained through the automatic search option in the FRESCO code [37] using the CC technique. The optimal set of the potential parameters deduced from the optical model fitting are then used as the initial values in the CC procedure fitting. The coupling schemes considered in the present paper are similar to what is sketched in Fig. 2 of Ref. [5].

IV. RESULTS AND DISCUSION

A. Analysis of the elastic data

To test the execute vibrations of α-particle clusters with respect to their most probable equilibrium positions at geometric bodies for the ^{20}Ne nucleus, we assume the cluster structure of ^{20}Ne as 5α (such as α density). At the same time, extension to the success of the structure model for ^{20}Ne density in Refs. [23–25] as two clusters, this distribution model is also considered in the present paper. In addition, the matter density distribution is taken as 2pF for the ^{20}Ne and ^{76}Ge nuclei.

The radial shape of the different types of the density distributions of ^{20}Ne is shown in Fig. 1, on linear and logarithmic scales. The corresponding rms radius calculated for ^{20}Ne (a cluster and 2pF) and ^{76}Ge nuclei (2pF) are listed in Table I in comparison with previous calculations and

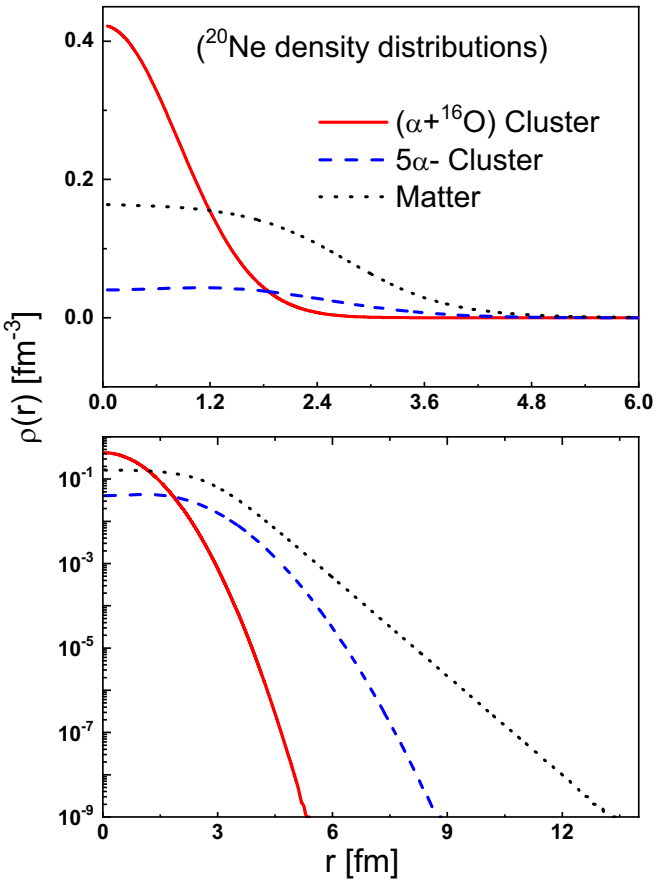

FIG. 1. Nuclear density distributions of the ^{20}Ne projectile; panel (a) for the linear scale and panel (b) for the logarithm scale. The solid line refers to the two cluster ($\alpha + {}^{16}$O) density distribution, the dashed line refers to the 5α distribution, whereas the dotted one represents the 2pF matter density form.

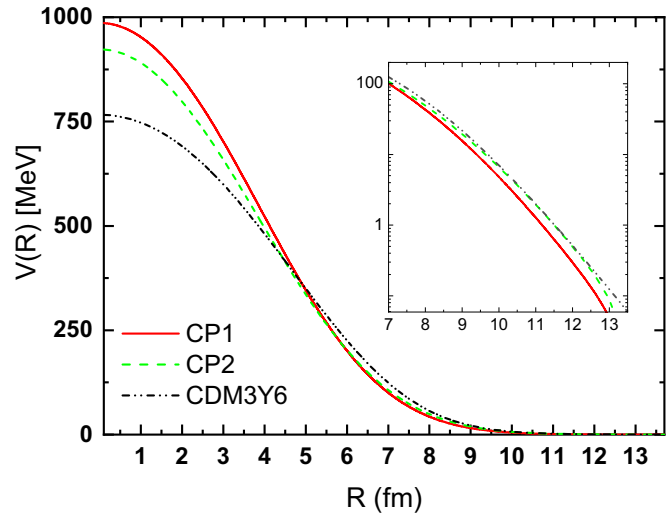

FIG. 2. The three OPs for ^{20}Ne + ^{76}Ge elastic scattering, CP1 (solid curve), CP2 (dashed curve), and CDM3Y6 (dashed-double dotted curve).

the experimental rms radius which are extracted using the relation $\langle r_{\rm m}^2\rangle^{1/2} = \langle r_{\rm ch}^2\rangle^{1/2} - \langle r_p^2\rangle^{1/2}$, where $r_{\rm ch}^2$ and r_p^2, respectively, are the charge density [19] and the proton rms radii. The features of the density distributions are shown in Fig. 1.

It can be seen that the two-cluster distribution has the largest value at the small distance ($r \leqslant 1$ fm) whereas the 5α distribution and 2pF densities have the same behavior with a small difference in the same region. For large r ($r > 1$ fm), the clearly difference between the considered densities is due to the different structure of the ^{20}Ne projectile nucleus. Generally, it is obvious from Fig. 1 that the cluster distributions have different behaviors than the nucleonic distributions. Moreover, the two-cluster distribution has a steeper slope than the 5α form.

The deduced values of the rms radius listed in Table I, together with the behavior of densities, shown in Fig. 1 leads us to say that the cluster structure ($\alpha + {}^{16}$O) of ^{20}Ne can play the function of deformation for the nucleus geometric structure. According to this hypothesis, the resulted CP1 and CP2 potential models will be affected.

The α-structure densities in addition to 2pF matter density forms of the ^{20}Ne nucleus with the considered NN effective interactions are investigated through the calculated DF potential. The three forms of the real part of the optical ^{20}Ne + ^{76}Ge potentials, CP1, CP2, and CDM3Y6 are shown in Fig. 2. It is obvious that the CP1 potential is deeper at a small radius whereas steeper than the other two potentials at a large radius which is relevant to the cluster structure of the ^{20}Ne nucleus. The behavior of the resulted potentials at a short distance is useless because of the dominance of the absorption behavior for the reaction. The difference between the folded potential is shown in the inset figure of Fig. 2 at the surface distances. This is mainly due to the peripheral nature of heavy-ion scattering at this range.

The experimental angular distribution of ^{20}Ne + ^{76}Ge elastic scattering at 306 MeV has been analyzed using the derived four potentials. The experimental data in comparison with the theoretical calculations are shown in Fig. 3. The best-fit parameters extracted from the autosearch processing in conjunction with real and imaginary volume integrals J_R ($J_{\rm W}$), rms radii, and the reaction cross section σ_R are listed in Table II. The listed parameters for the WSP potential are used as a guide for our calculations with respect to other work of the considered interaction [5]. One may note from Fig. 3 and Table II that all the derived potentials describe well the experimental data. It is obvious from this figure that the calculated cluster CP1 and CP2 potentials lead to successful predictions of the elastic scattering cross sections over all the measured angular range for the ^{20}Ne + ^{76}Ge system. Moreover, in the angular range $\theta \cong 12 - 17^\circ$, the CP1 and WSP potentials play almost the best fitting with the experimental data, smallest χ^2, and normalization scale factor close to one other than the other potentials (CP2 and CDM3Y6). For more confirmation of the obtained results, a different deal is taken to compare between the differential cross sections for the four considered potentials WSP, CP1, CP2, and CDM3Y6 where no real normalization (i.e., NR = 1.0) for the real potentials is taken and the imaginary WS parameters $W_0 = 84.3$,

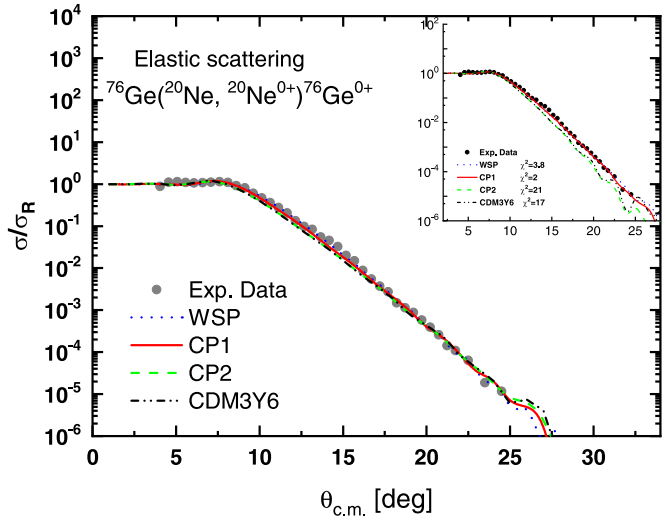

FIG. 3. A comparison between the measured elastic angular distribution [5] for ^{20}Ne + ^{76}Ge scattering at $E_{\text{lab.}} = 306$ MeV and the theoretical predictions obtained by using the optical CP1, CDM3Y6, and CP2 as well as WSP potentials as shown by solid, dashed-double dotted, dashed, and dotted lines, respectively. In the inset, fixed $N_r = 1.0$ with imaginary WS parameters are given inside the text.

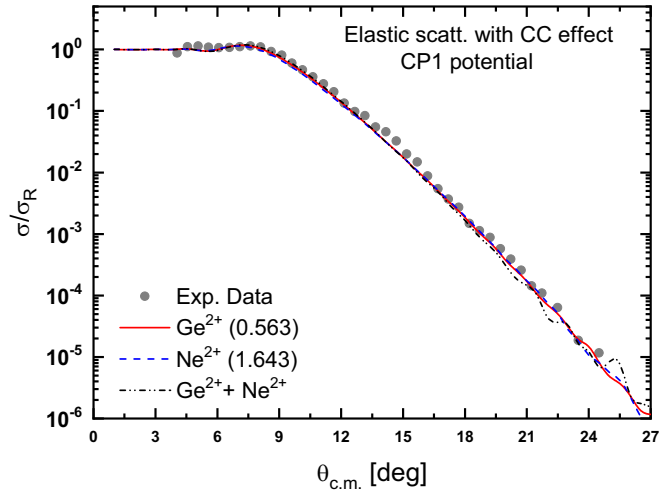

FIG. 4. The same as Fig. 3 but for the CP1 potential using the effect of CC calculations on elastic scattering. The solid line for the first low-lying excited states Ge^{+2} of target, the dashed line is for the first low-lying excited states of projectile Ne^{+2}, and the dashed-double dotted line refers to the mutual excitation (2^+, 2^+).

$a_w = 0.83$, and $r_w = 1.095$ are fixed for all the potentials. These results are shown in the inset of Fig. 3 with the corresponding χ^2 values. The smallest χ^2 for CP1 is obtained. The potentials CP1 and WSP still give the description of the experimental data. This presents one bonus for these two potentials to continue the description of the inelastic scattering using the CC technique.

This successful feature may be due to the cluster structure of the ^{20}Ne nucleus density distribution which confirms that the theoretical description of elastic scattering is sensitive to the structure of the two colliding nuclei. The present results are inconsistent with the previous study for Saptofora *et al.* [5]. They performed their calculations using three different OPs where all their chosen potentials failed to describe the elastic scattering data after the grazing angle (≈9.4°). This leads them to confirm that the theoretical description of elastic scattering is not strongly dependent on the choice of the OPs since the strong absorption restricts the reaction source on the colliding surface system.

To study the effect of adding the internal states of the projectile-target systems to elastic ^{20}Ne + ^{76}Ge scattering, the CC calculations are explicitly taken into account. The results of the deformed CP1 potential are shown in Fig. 4. Generally, negligible effects of CC are observed on the elastic scattering data. At large angles, a slightly effect of CC is noted for mutual excitation ^{20}Ne$_{1.634}(2^+)$ and ^{76}Ge$_{0.563}(2^+)$.

The resulting volume integrals are inconsistent with the previous one [5] also, the deduced values of the reaction cross-section (σ_R) are noted to be spread in a wider range ($\sigma_R = 3265 \pm 139.8$) in comparison with the previous one ($\sigma_R = 2808 \pm 10.1$). This refers to the dependence of cross-section values on the geometrical structure of the colliding nuclei.

B. Analysis of the inelastic scattering

For a deeper understanding of the scattering dynamics, the CC method where the relevant internal states of the projectile-target systems are explicitly taken into account, the theoretical calculations of angular distributions for the inelastic channels of the ^{20}Ne + ^{76}Ge system are performed.

To study the influence of different types of OPs, two different forms, CP1 and WSP are used to analyze the inelastic scattering data in the context of the CC approach. The effect of coupling is studied upon the elastic scattering cross section. The effect of couplings for the first low-lying excited states of projectile and target on the elastic channel is shown in Fig. 4. This figure substantiates the reliability of the CP1 cluster model.

The agreement with the data required to adjust the optical parameters by fitting the elastic and 2^+ inelastic curves in the CC calculations. This is performed separately for each nucleus in order to take into account the different coupling strengths. The obtained best-fit OP parameters are listed in Table III. The corresponding CP1 angular distribution calculations of inelastic scattering for ^{20}Ne$_{\text{g.s.}}(0^+)$ + ^{76}Ge$_{0.563}(2^+)$, and the mutually excited 2^+ states in both nuclei are shown in Fig. 5 compared to the experimental data and those extracted by the phenomenological WSP potential. It is obvious that a

TABLE III. The best-fit parameters for the WSP potential for CC calculations.

Excitation Mode	V_0 (MeV)	r_v (fm)	a_v (fm)	W_0 (MeV)	r_W (fm)	a_W (fm)	χ^2
^{76}Ge (2^+)	177.12	0.84	0.80	54.77	0.98	1.21	16.4
^{20}Ne (2^+)	177.84	0.86	0.95	14.39	1.34	0.79	1.50
(2^+, 2^+)	100.0	1.0	1.0	50.41	1.2	0.89	10.27

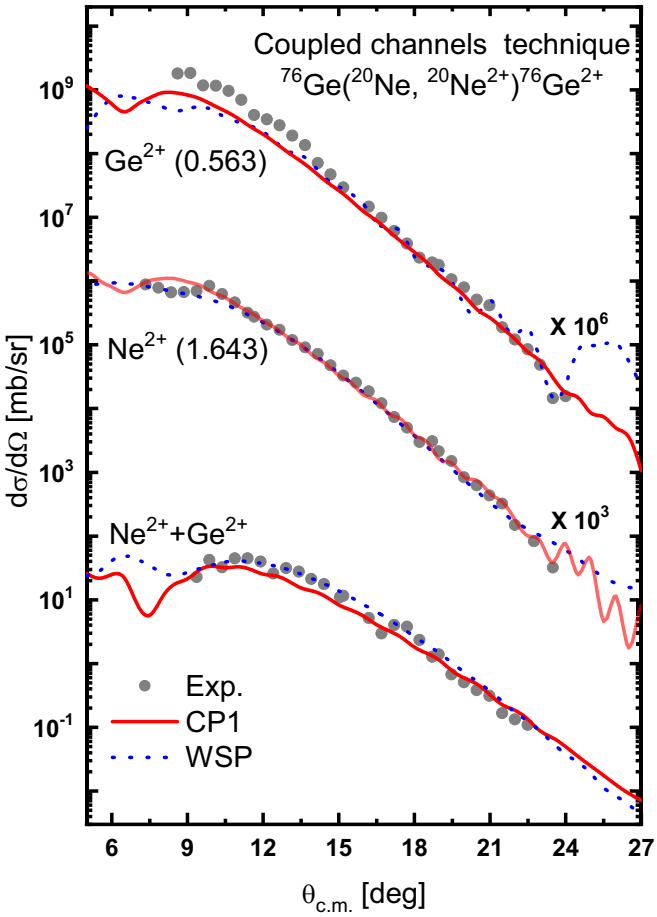

FIG. 5. The experimental angular distribution for the low-lying of projectile and target populated in the ^{20}Ne + ^{76}Ge inelastic scattering at 306 MeV in comparison to the theoretical CC calculations. The top data represent the 2^+ state of ^{76}Ge at 0.563 MeV; the middle data for the 2^+ state of ^{20}Ne at 1.634 MeV; the bottom data correspond to the excitation of both projectile and target ($2^+ \oplus 2^+$). The solid lines are the results of the CP1 potential whereas the dotted lines are the results of the WSP potential. Experimental data are taken from Ref. [5].

satisfactory agreement is obtained. The best-fit parameters of the imaginary WS part that is required to fit the CC calculations are listed in Table IV with $N_r = 0.8$. Generally, these results for all states, ^{20}Ne$_{1.634}(2^+)$, ^{76}Ge$_{0.563}(2^+)$ and the mutual excitation are better than that presented in Ref. [5]. Moreover, the resulted normalization factor N_R together with the χ^2 values indicate to the success the present calculations.

TABLE IV. The best-fit parameters of the imaginary WS part that required to fit the CC calculations with $N_r = 0.8$.

Nucleus	W_0 (MeV)	r_W (fm)	a_W (fm)	χ^2
^{76}Ge (2^+)	14.45	1.39	0.77	10.3
^{20}Ne (2^+)	50.15	1.21	0.83	3.3
(2^+, 2^+)	50.41	1.2	0.7	9.3

The satisfactory description for inelastic data may be due to the success of using cluster potential CP1 model to reproduce the elastic data for considered system.

The relative differences in the density and potential radii [33] are considered. Therefore, the deformation length ($\delta_\lambda^{\rm corr}$) that is adopted to match the deformed potential radii is used in this paper as Eq. (19). In contrast, indefinite deformation lengths for deformed nuclei are used in the previous study [5].

V. CONCLUSIONS

In the present paper, we have presented a successful description of the recently measured data for elastic and inelastic scattering of ^{20}Ne + ^{76}Ge at 306 MeV using the phenomenological WSP in addition to different three real OPs. The (α + ^{16}O)-cluster structure for the ^{20}Ne nucleus is considered to generate the real two-cluster CP1 potential in the optical form. Also, the 5α-cluster structure for ^{20}Ne is used to deduce the real potential. Moreover, the microscopic potential based upon the effective CDM3Y6 Paris NN interaction is also constructed. The imaginary part of all the derived potentials is used as a phenomenological WS form. The derived potentials reveal a very good agreement with the experimental elastic scattering angular distribution with a normalization factor close to unity.

In the framework of the CC technique, the inelastic scattering data are analyzed through two optical potentials, the two-cluster CP1 and phenomenological WSP. The coupling contribution from the first low-lying excited states 2^+ ($E_{\rm ex.}$ = 0.563 MeV) for the target and 2^+ ($E_{\rm ex.}$ = 1.634 MeV) for the projectile in addition to mutual excitations (2^+, 2^+) are considered. Very satisfactory reproduction of the inelastic and elastic data is obtained for all considered OPs. The effect of the CC on the elastic data is found to be negligible. These good results imply the success of the (α + ^{16}O)-cluster model for ^{20}Ne to analyze the considered DCE reaction which is an extension for the success of the previous studies in using this cluster structure [23–25].

More deeply, we can argue that the suggested cluster structure of the ^{20}Ne nucleus may present an internal distortion that makes the nucleus behave, such as a deformed nucleus. This change in the nucleus geometrical shape leads to the potential to be more sensitive at the surfaces of the colliding systems. Also, the α space configuration shape is accepted physically more than presented in the work of Spatafora *et al.* [5] where changing the radius is important to correctly describe the experimental data up to about 14° only. Furthermore, the extracted volume integrals and σ_R are found to be inconsistent with the only available previous study which requests another analysis of the considered system to be available to enable further discussion.

ACKNOWLEDGMENTS

This work was produced with the financial support of the Academy of Scientific Research and Technology (ASRT) of Egypt; ScienceUP/GradeUp initiative: Grant Agreement No. (6441). Its contents are the sole responsibility of the authors

and not necessary reflect the views of the Academy of Scientific Research and Technology. We are grateful to A. Saptofora for supporting the experimental data for the studied nuclear system. Also, we are indebted to A. Moro for his kind communication concerning the FRESCO code. The first author A.H. thanks Prof. F. Cappuzzello for the useful discussion.

[1] F. Cappuzzello, C. Agodi, M. Cavallaro, D. Carbone, S. Tudisco, D. Lo Presti, J. R. B. Oliveira, P. inocchiaro, M. Colonna, D. Rifuggiato *et al.*, Eur. Phys. J. A **54**, 72 (2018).
[2] F. Cappuzzello, C. Agodi, M. Bondì, D. Carbone, M. Cavallaro, and A. Foti, J. Phys.: Conf. Ser. **630**, 012018 (2015).
[3] H. Matsubara, M. Takaki, T. Uesaka, S. Shimoura *et al.*, Few-Body Syst. **54**, 1433 (2013).
[4] K. Kisamori, S. Shimoura, H. Miya, S. Michimasa *et al.*, Phys. Rev. Lett. **116**, 052501 (2016).
[5] A. Spatafora, F. Cappuzzello, D. Carbone *et al.*, Phys. Rev. C **100**, 034620 (2019).
[6] G. R. Satchler and W. G. Love, Phys. Rep. **55**, 183 (1979).
[7] G. Bertsch, J. Borysowicz, H. McMsnus, and W. G. Love, Nucl. Phys. A **284**, 399 (1977).
[8] D. T. Khoa and W. von Oertzen, Phys. Lett. B **304**, 8 (1993).
[9] D. T. Khoa, W. von Oertzen, and H. G. Bohlen, Phys. Rev. C **49**, 1652 (1994).
[10] D. T. Khoa, G. R. Satchler, and W. von Oertzen, Phys. Rev. C **56**, 954 (1997).
[11] D. T. Khoa, N. H. Phuc, D. T. Loan, and B. Minh, Phys. Rev. C **94**, 034612 (2016).
[12] D. T. Khoa, W. von Oertzen, H. G. Bohlen, and S. Ohkubo, J. Phys. G: Nucl. Part. Phys. **34**, R111 (2007).
[13] Kassem O. Behairy *et al.*, Chin. Phys. C **45**, 024101 (2021).
[14] M. El-Azab Farid, Z. M. M. Mahmoud, and G. S. Hassan, Nucl. Phys. A **691**, 671 (2001).
[15] M. A. Hassanain, A. A. Ibraheem, and M. El-Azab Farid, Phys. Rev. C **77**, 034601 (2008).
[16] M. A. Hassanain, A. A. Ibraheem, S. M. M. Al Sebiey, S. R. Mokhtar, M. A. Zaki, Z. M. M. Mahmoud, K. O. Behairy, and M. El-Azab Farid, Phys. Rev. C **87**, 064606 (2013).
[17] M. El-Azab Farid, A. A. Ibraheem, J. H. Al-Zahrani, W. R. Al-Harbi, and M. A. Hassanain, J. Phys. G: Nucl. Part. Phys. **40**, 075108 (2013).
[18] M. A. Hassanain, M. Anwar, and Kassem O. Behairy, Phys. Rev. C **97**, 044610 (2018).
[19] Z. M. M. Mahmoud, K. O. Behairy *et al.*, J. Phys. Soc. Jpn. **88**, 024201 (2019).
[20] B. Buck, C. B. Dover, and J. P. Vary, Phys. Rev. C **11**, 1803 (1975); B. Buck, A. C. Merchant, and S. M. Perez, *ibid.* **51**, 551 (1995); B. Buck, J. C. Johnston, A. C. Merchant, and S. M. Perez, *ibid.* **52**, 1840 (1995).
[21] Y. A. Berezhnoy and V. P. MikhaÏlyuk, Phys. At. Nucl. **63**, 715 (2000).
[22] P.-T. Ong, Y.-X. Yang, and Q.-R. Li, Eur. Phys. J. A **41**, 229 (2009).
[23] Y.-X. Yang, H.-L. Tan, and Q.-R. Li, Phys. Rev. C **82**, 024607 (2010).
[24] Y.-X. Yang and Q.-R. Li, Phys. Rev. C **84**, 014602 (2011).
[25] Y. Yang, X. Zhang, and Q. Li, J. Phys. G: Nucl. Part. Phys. **42**, 015101 (2015).
[26] H. de Vries, C. W. de Jager, and C. de Vries, At. Data Nucl. Data Tables **36**, 495 (1987).
[27] Z. M. M. Mahmoud and K. O. Behairy, Braz. J. Phys. **47**, 189 (2017).
[28] D. T. Khoa, W. von Oertzen, Phys. Lett. B **342**, 6 (1995); D. T. Khoa, W. von Oertzen, H. G. Bohlen, G. Bartnitzky, H. Clement, Y. Sugiyama, B. Gebauer, A. N. Ostrowski, Th. Wilpert, M. Wilpert, and C. Langner, Phys. Rev. Lett. **74**, 34 (1995).
[29] Z. Gao-Long, L. Hao, and L. Xiao-Yun, Chin. Phys. B **18**, 136 (2009).
[30] B. Pritychenko, M. Birch, B. Singh, and M. Horoi, At. Data Nucl. Data Tables **107**, 1 (2016).
[31] D. T. Khoa and G. Satchler, Nucl. Phys. A **668**, 3 (2000).
[32] G. R. Satchler, *Direct Nuclear Reactions* (Oxford University Press, Oxford, 1983).
[33] D. Carbone, R. Linares, P. Amador-Valenzuela, S. Calabrese, F. Cappuzzello *et al.*, Universe **7**, 58 (2021).
[34] D. T. Khoa, computer program DFPD4 (private communication).
[35] A. Hemmdan,M. A. Hanssanian, M. Anwar, and K. O. Behairy (unpublished).
[36] N. M. Clarke, HI-OPTIM 94.2 Code (private communication, 1994).
[37] I. J. Thompson, Comput. Phys. Rep. **7**, 167 (1988).